

## THE CHANGING AGN POPULATION

A. T. STEFFEN,<sup>1</sup> A. J. BARGER,<sup>1,2,3</sup> L. L. COWIE,<sup>3</sup> R. F. MUSHOTZKY,<sup>4</sup> Y. YANG<sup>4,5</sup>Accepted by *The Astrophysical Journal Letters*

## ABSTRACT

We investigate how the fraction of broad-line sources in the AGN population changes with X-ray luminosity and redshift. We first construct the rest-frame hard-energy (2 – 8 keV) X-ray luminosity function (HXLF) at  $z = 0.1 – 1$  using *Chandra* Lockman Hole-Northwest wide-area data, *Chandra* Deep Field-North 2 Ms data, other *Chandra* deep field data, and the *ASCA* Large Sky Survey data. We find that broad-line AGNs dominate above  $\sim 3 \times 10^{43}$  ergs s<sup>-1</sup> and have a mean luminosity of  $1.3 \times 10^{44}$  ergs s<sup>-1</sup>. Type II AGNs can only become an important component of the X-ray population at Seyfert-like X-ray luminosities. We then construct  $z = 0.1 – 0.5$  and  $z = 0.5 – 1$  HXLFs and compare them with both the local HXLF measured from *HEAO-1* A2 survey data and the  $z = 1.5 – 3$  HXLF measured from soft-energy (0.5 – 2 keV) *Chandra* and *ROSAT* data. We find that the number density of  $L_x > 10^{44}$  ergs s<sup>-1</sup> sources (quasars) steadily declines with decreasing redshift, while the number density of  $L_x = 10^{43} – 10^{44}$  ergs s<sup>-1</sup> sources peaks at  $z = 0.5 – 1$ . Strikingly, however, the number density of broad-line AGNs remains roughly constant with redshift while their average luminosities decline at the lower redshifts, showing another example of cosmic downsizing.

*Subject headings:* cosmology: observations — galaxies: evolution — galaxies: formation — galaxies: active

## 1. INTRODUCTION

It is becoming increasingly clear that low-redshift accretion may be the dominant phase of supermassive black hole (SMBH) growth (Barger et al. 2001; Cowie et al. 2003). Although theoretical models of SMBH formation have relied on comparisons with the optical quasar luminosity function, optically accessible broad-line active galactic nuclei (AGNs) form only about 30% (Barger et al. 2003b) of the X-ray background (XRB). Explanations for the lack of broad lines in most AGN optical spectra include absorption along the line-of-sight or dilution of the emission-line signatures by stellar light (Moran, Filippenko, & Chornock 2002). Regardless of the reason, optically and soft X-ray selected samples substantially undercount the AGN population relative to hard X-ray selected samples, at least at intermediate luminosities (Cowie et al. 2003; Barger et al. 2003a).

The hardest band for which the hard X-ray luminosity function (HXLF) can presently be determined is rest-frame 2 – 8 keV. The  $\approx 2$  Ms exposure of the *Chandra* Deep Field-North (CDF-N) samples a large, distant cosmological volume down to a very faint hard X-ray flux limit ( $f_{2-8 \text{ keV}} \approx 1.4 \times 10^{-16}$  ergs cm<sup>-2</sup> s<sup>-1</sup>; Alexander et al. 2003). However, this is substantially fainter than the X-ray flux of the sources that contribute the most to the XRB (Cowie et al. 2002), and the low-redshift volume sampled is small. To sample a large cosmological volume at low redshifts, we have mapped with *Chandra* an  $\sim 0.4$  deg<sup>2</sup> area in the Lockman Hole-Northwest (LH-NW) field to a flux level of  $f_{2-8 \text{ keV}} \approx 3 \times 10^{-15}$  ergs cm<sup>-2</sup> s<sup>-1</sup> (Yang et al. 2003), where most of the hard XRB is resolved. In this paper we

use our LH-NW data, together with deep *Chandra* data on the CDF-N, A370, SSA13, and SSA22 fields and bright *ASCA* data from Akiyama et al. (2000), to construct rest-frame 2 – 8 keV luminosity functions at low redshifts. We then investigate the evolution with redshift of AGN populations separated by optical spectral type. We assume  $\Omega_M = 1/3$ ,  $\Omega_\Lambda = 2/3$ , and  $H_o = 65$  km s<sup>-1</sup> Mpc<sup>-1</sup>. We use  $L_x$  to denote the rest-frame 2 – 8 keV luminosity.

## 2. X-RAY SAMPLE SELECTION

The LH-NW data are taken from the X-ray and optical catalogs of Y. Yang et al. (in preparation) and A. T. Steffen et al. (in preparation). Here we consider only sources with fluxes above  $5 \times 10^{-16}$  ergs cm<sup>-2</sup> s<sup>-1</sup> (0.5 – 2 keV) and  $5 \times 10^{-15}$  (2 – 8 keV) to provide good, high-significance samples. We also only consider those sources that have been targeted spectroscopically. The only source property we considered when making our masks for spectroscopy was X-ray flux (sources with higher X-ray fluxes had higher priority when we had to choose one X-ray source over another due to mask conflicts). We spectroscopically observed 150 sources out of our total 2 – 8 keV sample of 228. We were able to confidently identify 100 of these 150 sources (67%) based on multiple emission and/or absorption line features. Two of the identified sources are stars. A practical optical limit for obtaining redshifts for X-ray sources using the Deep Extragalactic Imaging Multi-Object Spectrograph (DEIMOS; Faber et al. 2002) on Keck II is about  $R = 24$  (see Barger et al. 2003b). Other spectra may not have been identifiable due to slits falling too close to an edge of the CCD or bright neighbor

<sup>1</sup>Department of Astronomy, University of Wisconsin-Madison, 475 North Charter Street, Madison, WI 53706.

<sup>2</sup>Department of Physics and Astronomy, University of Hawaii, 2505 Correa Road, Honolulu, HI 96822.

<sup>3</sup>Institute for Astronomy, University of Hawaii, 2680 Woodlawn Drive, Honolulu, Hawaii 96822.

<sup>4</sup>Laboratory for High Energy Astrophysics, Goddard Space Flight Center, Code 660, NASA, Greenbelt, MD, 20770.

<sup>5</sup>Department of Astronomy, University of Maryland, College Park, MD, 20742.

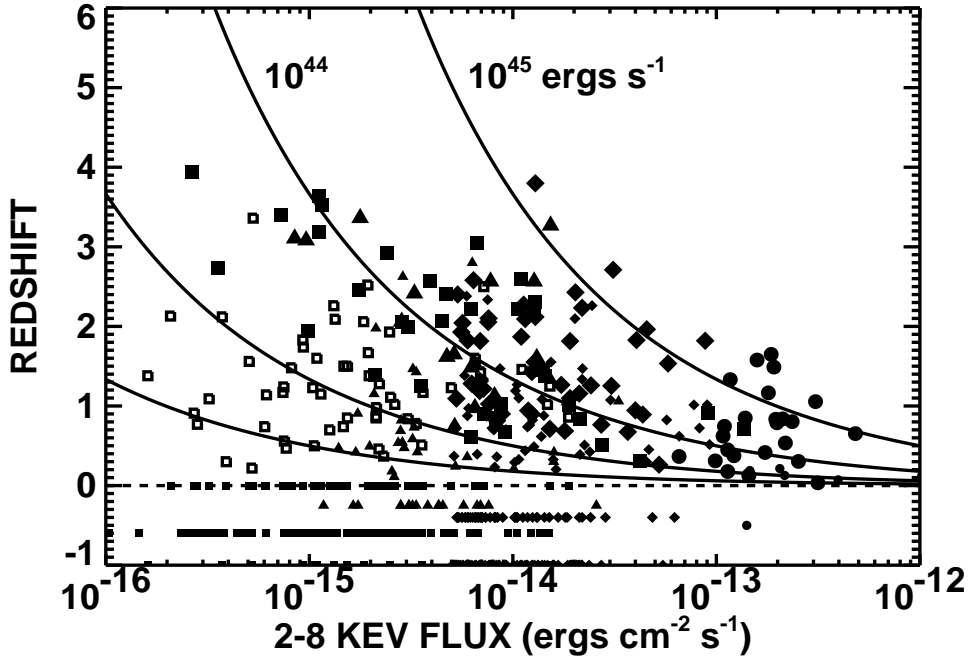


FIG. 1.— Redshift (solid for spectroscopic, open for photometric) vs. 2 – 8 keV flux for the X-ray samples (*squares*—CDF-N; *triangles*—A370, SSA13, and SSA22; *diamonds*—LH-NW; *circles*—*ASCA*). Broad-line optical spectra are denoted by large solid symbols. Unidentified sources are denoted by small solid symbols at  $z < 0$ . Solid curves show flux vs. redshift for  $L_x = 10^{42}$  ergs  $s^{-1}$  (lowest curve),  $10^{43}$ ,  $10^{44}$ , and  $10^{45}$  (highest curve), computed with a  $K$ -correction for a  $\Gamma = 1.8$  power law spectrum (see Barger et al. 2002).

objects compromising the spectra.

The faintest X-ray data are taken from the  $\approx 2$  Ms CDF-N catalogs of Alexander et al. (2003; X-ray) and Barger et al. (2003b; optical). Excluding stars and the small number of extended X-ray sources, the 2 – 8 keV sample contains 326 sources, 68% of which have either spectroscopic (165) or reliable photometric (56) redshifts. Our other *Chandra* and *ASCA* samples are summarized in Cowie et al. (2003). Hereafter, we refer to the A370, SSA13, and SSA22 *Chandra* samples collectively as “other”.

In our analysis we place every X-ray source that was not spectroscopically identified for any reason into each and every redshift interval in order to obtain a strict upper bound on the number of AGNs that could lie in that redshift interval, modulo the existence of a substantial population of Compton-thick sources not detected by *Chandra*. We note in passing that Barger et al. (2002) found from the 1 Ms CDF-N data that a substantial population of Compton-thick sources is not needed to explain the greater than 8 keV XRB, provided that the *ASCA* and *BeppoSAX* XRB measurements, instead of the lower *HEAO-1* A2 measurement, are assumed at energies less than 8 keV. For the LH-NW field, we only ever consider the sources that were spectroscopically observed (identified or not). This is acceptable because the spectroscopy are purely from targeted observations of the X-ray samples. For the other fields, the spectroscopy are not purely from targeted observations of the X-ray samples, so we need to include all of the sources.

We determined the solid angle covered by the combined samples at a given flux by comparing the observed

numbers of sources versus flux with the averaged number counts in the 2 – 8 keV band from Cowie et al. (2002). This method allows a simple treatment of the incompleteness that was modeled in computing the counts. However, the counts in Cowie et al. also include the low CDF-S counts, which may affect the normalization at the 10% level relative to the LH-NW average (Yang et al. 2003). We consider this to be a reasonable estimate of the systematic errors in the present analysis. The solid angle covered by the combined 2 – 8 keV samples ranges from  $0.002 \text{ deg}^2$  at the faintest fluxes to  $5.8 \text{ deg}^2$  at the highest fluxes. At  $2.3 \times 10^{-14} \text{ ergs cm}^{-2} \text{ s}^{-1}$  (2 – 8 keV) the solid angle is  $0.52 \text{ deg}^2$ .

In Figure 1 we show redshift versus 2 – 8 keV flux for the *ASCA* (*circles*), LH-NW (*diamonds*), CDF-N (*squares*), and other (*triangles*) samples. The LH-NW sources nicely fill in the almost an order of magnitude flux gap between the CDF-N and *ASCA* samples. The solid curves correspond to loci of constant  $L_x$ . Any source more luminous than  $L_x = 10^{42}$  ergs  $s^{-1}$  is very likely to be an AGN on energetic grounds (Zezas, Georgantopoulos, & Ward 1998; Moran et al. 1999), though many of the intermediate luminosity sources do not show obvious AGN signatures in their optical spectra.

### 3. THE AGN X-RAY LUMINOSITY FUNCTION

Cowie et al. (2003) used *Chandra*, *ASCA*, and *ROSAT* data to determine rest-frame 2 – 8 keV AGN luminosity functions in two redshift intervals,  $z = 0.1$ –1 and  $z = 2$ –4. They did not have very many sources in their sample with 2 – 8 keV fluxes  $\sim 2 \times 10^{-14}$  to  $10^{-13} \text{ ergs cm}^{-2} \text{ s}^{-1}$  since

that intermediate flux range is not well covered by either small-area, deep *Chandra* observations or bright *ASCA* observations. With our wide-area LH-NW data, we now have good coverage of the intermediate flux range and can therefore improve the determination of the  $z = 0.1 - 1$  HXLF.

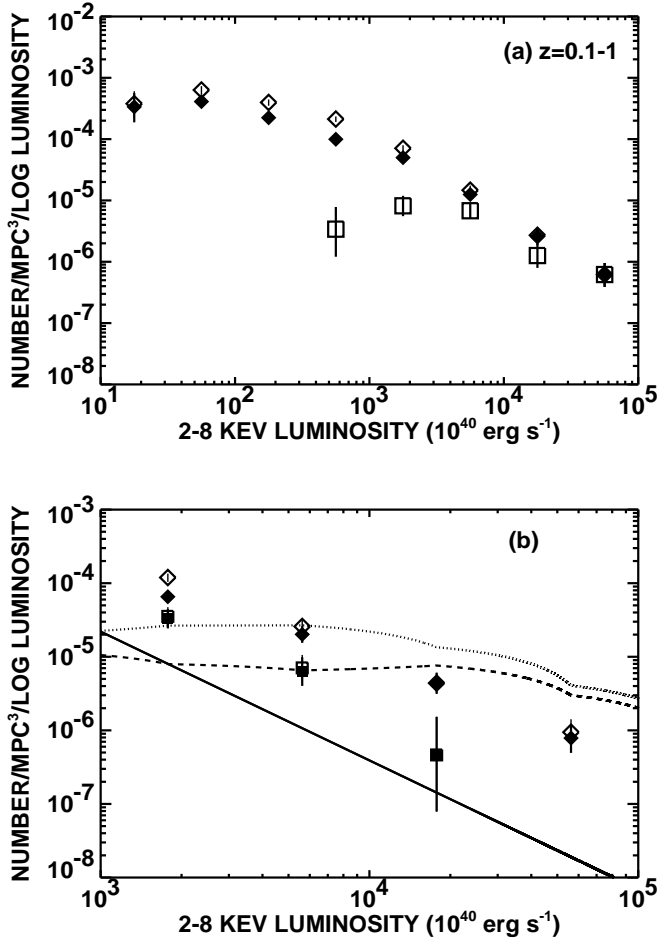


FIG. 2.— (a) Rest-frame 2 – 8 keV luminosity function per unit logarithmic luminosity for  $z = 0.1 - 1$  (*solid diamonds*), computed from observed-frame 2 – 8 keV assuming an intrinsic  $\Gamma = 1.8$ , for which there are only small differential  $K$ -corrections to rest-frame 2 – 8 keV. No correction was made for intrinsic absorption, but in rest-frame 2 – 8 keV, average absorption corrections are small. Maximal  $z = 0.1 - 1$  HXLF (*open diamonds*) was found by assigning all of the unidentified sources redshifts at the volume-weighted centers of each and every redshift interval. True HXLF lies somewhere between the solid and open diamonds. Open squares show the  $z = 0.1 - 1$  HXLF for broad-line AGNs only. Poissonian  $1\sigma$  uncertainties are based on the number of sources in each logarithmic luminosity bin. (b) Rest-frame HXLF from (a) broken into two smaller redshift intervals,  $z = 0.1 - 0.5$  (*solid squares*) and  $z = 0.5 - 1$  (*solid diamonds*). Maximal HXLFs are shown with open symbols. The  $z = 1.5 - 3$  HXLF (*dashed line*; computed from observed-frame 0.5 – 2 keV) and the local Seyfert galaxy HXLF (*solid line*; from Piccinotti et al. 1982) are shown for comparison. Dotted line is maximal  $z = 1.5 - 3$  HXLF, found by assigning redshifts to all of the unidentified sources at the volume-weighted centers of each and every redshift interval. True  $z = 1.5 - 3$  HXLF lies somewhere between the dashed and dotted lines.

In Figure 2a we show our measured HXLF for the  $z = 0.1 - 1$  interval (*solid diamonds*), computed following Cowie et al. (2003), who used the traditional  $1/V_a$  method of Felten (1977). The uncertainties are Poissonian, based on the number of galaxies in each logarithmic luminosity

bin. However, since incompleteness is a potentially larger source of error, we also recomputed the HXLF (*open diamonds*) by assigning all of the unidentified sources to the volume-weighted centers of each and every redshift interval. Because the spectroscopic identifications are much more complete at the high X-ray fluxes, the associated systematic uncertainties are larger at low  $L_x$ . The HXLF of only the broad-line AGNs is shown by the large open squares in Figure 2a. In the high luminosity range where the HXLF is steep, we can see that the broad-line AGNs dominate the total HXLF.

The uncorrected  $z = 0.1 - 1$  HXLF can be well represented by a conventional broken power law fit of the form  $6.6 \times 10^{-6} L_{44}^{-1.37}$  per  $\text{Mpc}^3$  above  $2 \times 10^{43} \text{ ergs s}^{-1}$  and  $1.5 \times 10^{-5} L_{44}^{-0.87}$  below, where  $L_{44}$  is the luminosity in units of  $10^{44} \text{ ergs s}^{-1}$ . The integrated  $z = 0.1 - 1$  light density is  $1.8 \times 10^{39} \text{ ergs s}^{-1} \text{ Mpc}^{-3}$ . Half of the total uncorrected light in the  $z = 0.1 - 1$  interval arises in sources more luminous than  $2.1 \times 10^{43} \text{ ergs s}^{-1}$ , and about one-third arises in broad-line AGNs.

In Figure 2b we show our measured HXLF over the luminosity range  $L_x = 10^{43}$  to  $10^{45} \text{ ergs s}^{-1}$ , where most of the sources have been spectroscopically identified, divided into two smaller redshift intervals,  $z = 0.1 - 0.5$  (*squares*) and  $z = 0.5 - 1$  (*diamonds*). For comparison, we show the local Seyfert galaxy HXLF (*solid line*) from Piccinotti et al. (1982; converted to  $H_0 = 65 \text{ km s}^{-1} \text{ Mpc}^{-1}$  and, using their assumed  $\Gamma = 1.7$ , to 2 – 8 keV) and the high-redshift HXLF (*dashed line*) from Cowie et al. (2003; updated to include our LH-NW data and the 2 Ms CDF-N data, and to cover the interval  $z = 1.5 - 3$ ). We have computed the maximal high-redshift HXLF (*dotted line*) by assigning all of the unidentified sources to the volume-weighted centers of each and every redshift interval. The high-redshift HXLF is much tighter than in Cowie et al. (2003) because of our slightly lower redshift interval and our higher spectroscopic completeness. From Figure 2b we see that the number density of  $L_x > 10^{44} \text{ ergs s}^{-1}$  sources steadily declines with decreasing redshift. However, the number density of  $L_x = 10^{43} - 10^{44} \text{ ergs s}^{-1}$  sources is largest in the  $z = 0.5 - 1$  interval and smaller at both higher and lower redshifts (see also Fig. 4).

#### 4. X-RAY FLUXES AND LUMINOSITIES

Prior to *Chandra* and *XMM-Newton*, various groups (e.g., Comastri et al. 1995; Gilli, Salvati, & Hasinger 2001) using XRB population synthesis models based on unified AGN schemes predicted that a mixture of unobscured type I AGNs and intrinsically obscured type II AGNs were needed to produce the bulk of the XRB. The obscured systems were expected to lie at high redshifts ( $z = 2 - 3$ ), with the high luminosity end (type II quasars) contributing substantially to the XRB. Contrary to the predictions, optical observations of the sources detected in deep *Chandra* and *XMM-Newton* hard X-ray surveys have found a redshift distribution that peaks at  $z < 1$  (Barger et al. 2002, 2003b; Hasinger 2003). Only a handful of type II quasars (here we define quasars as having  $L_x > 10^{44} \text{ ergs s}^{-1}$ ) have been detected, and these contribute only a small fraction of the XRB (e.g., Barger et al. 2003b).

In Figure 3 we plot for the redshift intervals  $z = 0.1 - 1$  and  $z = 1.5 - 3$  the fractional number of X-ray sources in

each luminosity bin, by optical spectral type, versus rest-frame 2–8 keV luminosity. From Figure 3a we see that the dominant population at quasar luminosities, where our redshift identifications are very complete, is broad-line AGNs. However, at more Seyfert-like luminosities ( $L_x < 10^{44}$  ergs s $^{-1}$ ), the broad-line AGN fraction declines rapidly with decreasing luminosity. Figure 3b shows a similar trend with luminosity. These results suggest a luminosity dependence in optical spectral type: type I AGNs dominate at quasar luminosities, while type II AGNs can only become an important component of the X-ray population at Seyfert-like luminosities.

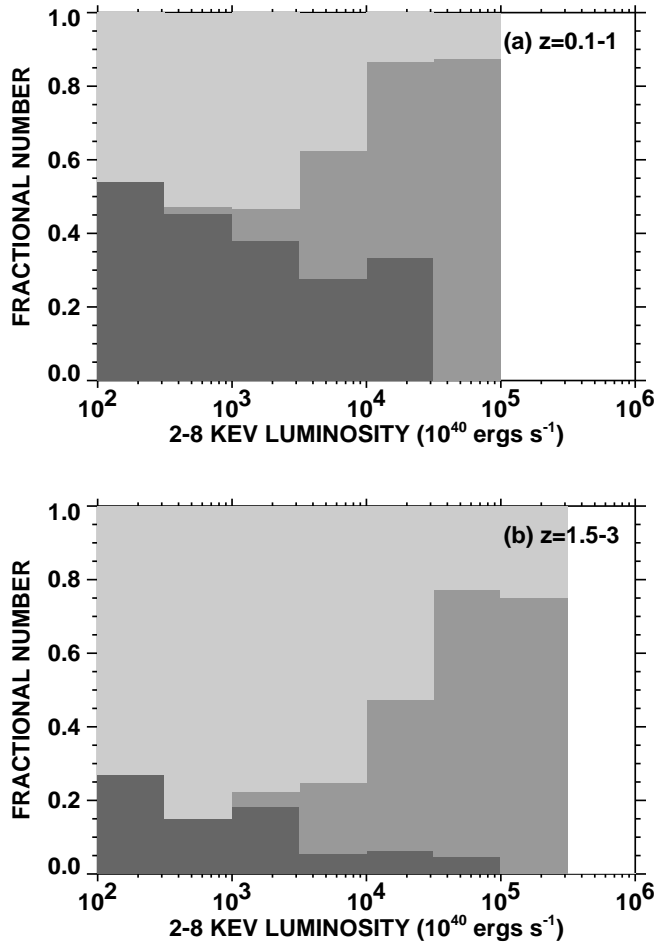


FIG. 3.— Fractional number of X-ray sources by optical spectral type (dark shading—non-broad-line sources; medium shading—broad-line AGNs; light shading—unidentified sources) versus 2–8 keV luminosity for the redshift intervals (a)  $z = 0.1 - 1$  and (b)  $z = 1.5 - 3$ . Luminosities were computed with a  $K$ -correction for a  $\Gamma = 1.8$  power law spectrum. All of the unidentified sources were assigned redshifts at the volume-weighted centers of each and every redshift interval.

To quantify this, we note that in the  $z = 0.1 - 1$  redshift interval there are 20 sources with quasar luminosities, of which 15 are broad-line AGNs. Only three of the unidentified sources would have quasar luminosities if placed in this redshift interval, so the systematic errors are small, and the bulk of the quasars are broad-line AGNs. In the  $z = 1.5 - 3$  interval there are 65 sources with quasar luminosities, of which 58 are broad-line AGNs. There are 56 unidentified sources that would have quasar luminosities

if placed in this redshift interval, so the systematic uncertainties are larger. However, at least half (and probably considerably more) of the sources with quasar luminosities in this redshift interval are broad-line AGNs.

## 5. DISCUSSION

Barger et al. (2003a) graphically showed how the  $L_x = 10^{43} - 10^{44}$  ergs s $^{-1}$  (Seyfert-like luminosities) number density slowly increases with decreasing redshift from  $z = 6$  to  $z = 0.1$ , while the  $L_x = 10^{44} - 10^{45}$  ergs s $^{-1}$  (quasar luminosities) number density peaks at  $z = 1.5 - 3$ . They also showed that the evolution of the  $L_x = 10^{44} - 10^{45}$  ergs s $^{-1}$  number density closely matches in shape the evolution of optically selected quasars. Given these trends and our interesting result from Figure 3 that while the dominant population at quasar luminosities is broad-line AGNs, at lower luminosities the broad-line fraction drops dramatically, here we explore a different aspect of the number density evolution.

In Figure 4 we show number density versus redshift for the sources with  $L_x > 10^{43}$  ergs s $^{-1}$ . Rather than dividing the sources into luminosity classes, as was done in Barger et al. (2003a), we have instead divided the sources into broad-line (*open squares*) and non-broad-line (*solid circles*) AGNs. The horizontal bars show the maximal number densities for the non-broad-line AGNs, obtained by assigning all of the unidentified sources redshifts at the volume-weighted centers of each and every redshift bin and then retaining only those with  $L_x > 10^{43}$  ergs s $^{-1}$ . The bars are not consistent with one another because all of the unidentified sources are included in each and every redshift bin, as long as their luminosities at those redshifts exceed  $10^{43}$  ergs s $^{-1}$ .

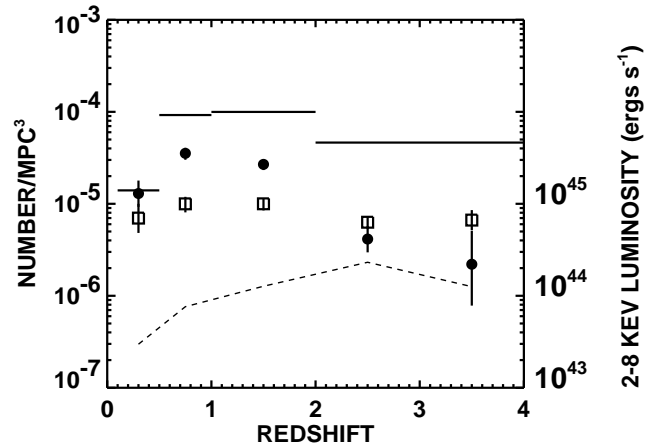


FIG. 4.— Number density of sources with  $L_x > 10^{43}$  ergs s $^{-1}$  vs. redshift. Broad-line (non-broad-line) AGNs are denoted by open (solid) symbols. Points above (below)  $z = 2$  were determined from observed-frame 2–8 keV (0.5–2 keV), assuming an intrinsic  $\Gamma = 1.8$ . Poissonian  $1\sigma$  uncertainties are based on the number of sources in each redshift bin. Horizontal bars show the maximal number densities for the non-broad-line AGNs, found by assigning redshifts to all of the unidentified sources at the volume-weighted centers of each and every redshift bin and then retaining only those with  $L_x > 10^{43}$  ergs s $^{-1}$ . Dashed line shows the mean luminosity (right-hand axis) of the broad-line AGNs with redshift.

From Figure 4 we see that the number density of non-broad-line AGNs with  $L_x > 10^{43}$  ergs s $^{-1}$  rises with de-

creasing redshift, until the last redshift bin. Strikingly, however, the number density of broad-line AGNs remains roughly constant with redshift while their average luminosities (*dashed line; right-hand axis*) decline at the lower redshifts. This is another example of cosmic downsizing. In the terminology of previous quasar studies, the broad-line AGNs are undergoing pure luminosity evolution, not density evolution. Pure luminosity evolution is consistent with the most recent optical determinations (Boyle et al. 2000). The increase in the number density of non-broad-line sources and the decrease in the broad-line AGN average luminosities results in non-broad-line sources increasingly dominating the light at lower redshifts, modulo

the existence of a substantial population of Compton-thick sources.

We gratefully acknowledge support from NASA's National Space Grant College and Fellowship Program and the Wisconsin Space Grant Consortium (A. T. S.), CXC grants GO2-3191A (A. J. B.) and GO2-3187B (L. L. C.), NSF grants AST-0084847 (A. J. B.) and AST-0084816 (L. L. C.), the University of Wisconsin Research Committee with funds granted by the Wisconsin Alumni Research Foundation (A. J. B.), the Alfred P. Sloan foundation (A. J. B.), and the IDS program of R. F. M.

## REFERENCES

- Akiyama, M., et al. 2000, *ApJ*, 532, 700  
 Alexander, D. M., et al. 2003, *AJ*, 126, 539  
 Barger, A. J., Cowie, L. L., Bautz, M. W., Brandt, W. N., Garmire, G. P., Hornschemeier, A. E., Ivison, R. J., & Owen, F. N. 2001, *AJ*, 122, 2177  
 Barger, A. J., Cowie, L. L., Brandt, W. N., Capak, P., Garmire, G. P., Hornschemeier, A. E., Steffen, A. T., & Wehner, E. H. 2002, *AJ*, 124, 1839  
 Barger, A. J., Cowie, L. L., Capak, P., Alexander, D. M., Bauer, F. E., Brandt, W. N., Garmire, G. P., & Hornschemeier, A. E. 2003a, *ApJ*, 584, L61  
 Barger, A. J., et al. 2003b, *AJ*, 126, 632  
 Boyle, B. J., Shanks, T., Croom, S. M., Smith, R. J., Miller, L., Loaring, N., & Heymans, C. 2000, *MNRAS*, 317, 1014  
 Comastri, A., Setti, G., Zamorani, G., & Hasinger, G. 1995, *A&A*, 296, 1  
 Cowie, L. L., Barger, A. J., Bautz, M. W., Brandt, W. N., & Garmire, G. P. 2003, *ApJ*, 584, L57  
 Cowie, L. L., Garmire, G. P., Bautz, M. W., Barger, A. J., Brandt, W. N., & Hornschemeier, A. E. 2002, *ApJ*, 566, L5  
 Faber, S. M., et al. 2002, *Proc. SPIE*, 4841, 186  
 Felten, J. E. 1977, *AJ*, 82, 861  
 Gilli, R., Salvati, M., & Hasinger, G. 2001, *A&A*, 366, 407  
 Hasinger, G. 2003, in *The Emergence of Cosmic Structure*, eds. S. S. Holt & C. S. Reynolds, AIP Conf. Proc. 666, 227  
 Moran, E. C., Filippenko, A. V., & Chornock, R. 2002, *ApJ*, 579, L71  
 Moran, E. C., Lehnert, M. D., & Helfand, D. J. 1999, *ApJ*, 526, 649  
 Piccinotti, G., Mushotzky, R. F., Boldt, E. A., Holt, S. S., Marshall, F. E., Serlemitsos, P. J., & Shafer, R. A. 1982, *ApJ*, 253, 485  
 Yang, Y., Mushotzky, R. F., Barger, A. J., Cowie, L. L., Sanders, D. B., & Steffen, A. T. 2003, *ApJ*, 585, L85  
 Zezas, A., Georgantopoulos, I., & Ward, M. J. 1998, *MNRAS*, 301, 915